

Dirac-Hartree-Fock calculation of the $2^3S_1 \rightarrow 1^1S_0$ transition rates for the He isoelectronic sequence*

W. R. Johnson and Chien-ping Lin

Department of Physics, University of Notre Dame, Notre Dame, Indiana 46556

(Received 5 November 1973)

A new calculation of the $M1$ decay rates of the metastable 2^3S_1 states of two-electron ions is presented. The calculation is based on the Furry bound-interaction representation of quantum electrodynamics and expansion in powers of αZ is avoided. The basic one-electron states are constructed from solutions to the Dirac equation including the ground-state Dirac-Hartree-Fock potential. Correlation and transverse-photon-exchange effects, both of relative order Z^{-1} , are included in the calculation by the perturbation expansion of the S matrix in powers of α . Decay rates calculated to lowest order in powers of α are smaller than previously reported rates. When correlation and transverse-photon-exchange corrections are included in the calculation the resulting rates agree well with previous calculations. We estimate that the present values are more accurate than the older results for $Z > 12$, while for smaller Z the older results are expected to be better. The close agreement between the present calculations and previous theoretical results confirms the smallness of both higher-order relativistic effects and of higher-order correlation corrections in calculations of this type.

I. INTRODUCTION

During the past few years there has been renewed interest in the decay of metastable 2^3S_1 states of two-electron ions. This renewed interest stems from the identification of intense $2^3S_1 - 1^1S_0$ lines for several two-electron ions in the x-ray spectrum of the sun by Gabriel and Jordan.¹

Following the observation of the one-photon decays, several calculations of the corresponding $M1$ decay rates have appeared. The first of these recent calculations by Griem² made use of screened Dirac wave functions. More accurate calculations by Drake,³ by Feinberg and Sucher,⁴ and by Beigman and Safronova⁵ followed. In all three of these more accurate calculations, relativistic corrections of higher order (in powers of αZ) are omitted.

In addition to the theoretical work on the $M1$ decay rate a number of laboratory measurements have been reported by Schmieder and Marrus⁶ (Ar¹⁶⁺); Moos and Woodworth⁷ (He); Gould, Marrus, and Schmieder⁸ (Ar¹⁶⁺, Ti²⁰⁺); and Cocke, Curnutte, and Randall⁹ (Cl¹⁵⁺). The experimental lifetimes are all smaller than the theoretically predicted values. In the case of He, where the experimental errors are largest, the theoretical value is within the experimental error limits.

To determine whether this discrepancy between theory and experiment can be accounted for by those terms of higher order in αZ neglected in previous calculations, we have undertaken a relativistic evaluation of the $M1$ decay rates in which

expansion in a αZ is avoided.

Our point of departure is the Furry bound-interaction representation of quantum electrodynamics.¹⁰ In the Furry picture the electron-positron field operator $\psi(\vec{r}, t)$ is expanded in the complete set of solutions to the Dirac equation in the nuclear Coulomb field. For our purposes it is convenient to include the principal effect of the electron-electron interaction in the field operator ψ . To accomplish this we expand ψ in the complete set of solutions to the Dirac equation including the Dirac-Hartree-Fock (DHF) potential. This potential includes, together with the nuclear Coulomb field, the ground-state self-consistent potential. The inclusion of the self-consistent potential in ψ , and in the electron-positron Hamiltonian, requires the introduction of a DHF counter term in the interaction Hamiltonian.

To calculate the decay rate we employ the usual perturbation expansion of the S matrix. The lowest-order term in the perturbation expansion, $S^{(1)}$, gives a matrix element of order $(\alpha Z)^4$. The next nonvanishing term in the perturbation expansion, $S^{(3)}$, which includes the effects of one-photon exchange, gives a matrix element of order $\alpha(\alpha Z)^3$, or of order Z^{-1} relative to the lowest-order term. In evaluating $S^{(3)}$ we omit the contribution of electron self-energy and vacuum polarization which are expected to be considerably smaller than the one-photon exchange terms. The contributions of $S^{(5)}$ and higher-order terms in the S -matrix expansion, which are dominated by the Z^{-2} correlation corrections, are also omitted.

Since we include terms of relative order $(\alpha Z)^2$ in the present calculation but omit corrections of order Z^{-2} , we expect our results to be more accurate than previous theoretical values for large Z . A rough estimate of the range of Z for which the present calculations represent an improvement is given by assuming that the coefficients of the terms omitted in the present case (the Z^{-2} terms) and those omitted in previous calculations [the $(\alpha Z)^2$ terms] are equal. On this basis one judges that for $Z > \alpha^{-1/2} \approx 12$ the present values are more reliable.

These present results, which are given in Table I, are seen to be in substantial agreement with previous values represented by Drake's calculation³ for the entire range $2 \leq Z \leq 26$. One is led to the conclusion that the terms of higher order in αZ omitted previously are not responsible for the existing discrepancy between theory and experiment. Further, one may judge from the close agreement between the present calculation and the older results that an approximate treatment of correlation such as that presented here is sufficient for computing reliable decay rates, even for the lightest elements.

II. CONSTRUCTION OF THE DHF POTENTIAL AND ORBITALS

As mentioned in the Introduction, we wish to include effects of the electron-electron interaction as well as the electron-nucleus interaction in the electron-positron field operator $\psi(\vec{r}, t)$. To this end we expand $\psi(\vec{r}, t)$ in the complete set of DHF orbitals $u_{n\kappa m}$. These orbitals are solutions to the time-independent Dirac equation

$$\begin{aligned} [h_0 - \alpha Z(r)/r] u_{n\kappa m} &= \epsilon_{n\kappa m} u_{n\kappa m}, \\ h_0 &= \vec{\alpha} \cdot \vec{p} + \beta m, \end{aligned} \quad (2.1)$$

where $\vec{\alpha}$ and β are the usual Dirac matrices and where $\alpha Z(r)/r$ is a spherically symmetric potential introduced to account for the electron-electron interaction in the 1^1S_0 ground state, and for the electron-nucleus interaction.

The assumed spherical symmetry of $Z(r)$ permits an angular decomposition of the orbitals

$$u_{n\kappa m}(\vec{r}) = \frac{1}{r} \begin{pmatrix} iG_{n\kappa}(r)\Omega_{\kappa m}(\hat{r}) \\ F_{n\kappa}(r)\Omega_{-\kappa m}(\hat{r}) \end{pmatrix}. \quad (2.2)$$

The subscripts n , κ , and m are the usual principal and angular momentum quantum numbers, while $G_{n\kappa}(r)$ and $F_{n\kappa}(r)$ are the "large" and "small" component radial Dirac functions, and $\Omega_{\kappa m}(\hat{r})$ is a spherical spinor.

To simplify our notation somewhat we designate

the one-electron orbitals $1s_{1/2}$ and $2s_{1/2}$ by the subscripts 1 and 2. The effective charge $Z(r)$ introduced in Eq. (2.1) is given as $Z(r) = Z - Y(r)$, where the DHF screening function $Y(r)$ is defined by

$$Y(r) = \int_0^r dr (G_1^2 + F_1^2) + r \int_r^\infty \frac{dr}{r} (G_1^2 + F_1^2). \quad (2.3)$$

The radial functions $G_1(r)$ and $F_1(r)$ satisfy a pair of coupled differential equations which follow from Eqs. (2.1) and (2.2):

$$\begin{aligned} \left(\frac{d}{dr} + \frac{1}{r} \right) F_1 + \left(m - \epsilon_1 - \frac{\alpha Z(r)}{r} \right) G_1 &= 0, \\ \left(\frac{d}{dr} - \frac{1}{r} \right) G_1 + \left(m + \epsilon_1 + \frac{\alpha Z(r)}{r} \right) F_1 &= 0. \end{aligned} \quad (2.4)$$

The system of Eqs. (2.3) and (2.4) are solved self-consistently for $G_1(r)$, $F_1(r)$, and ϵ_1 . Once $Y(r)$ is known in terms of the self-consistent solutions, an entire spectrum including both positive and negative eigenvalues $\epsilon_{n\kappa m}$ can, in principle, be determined from Eq. (2.1). In Figs. 1 and 2 we show graphs of the numerically determined radial functions for the $1s_{1/2}$ and $2s_{1/2}$ orbitals in the special case $Z = 20$.

III. MODIFICATION OF THE FURRY BOUND-INTERACTION REPRESENTATION

To calculate the decay rate of a two-particle excited state we employ the Furry bound-interaction representation¹⁰ and the perturbation expansion of quantum electrodynamics. The ground-state DHF potential $\alpha Y(r)/r$ is included with the nuclear potential in the electron-positron Hamiltonian. We compensate for the above modification by subtracting an identical term from the interaction Hamiltonian H_{e-p} . The entire calculation is carried out, for convenience, in the Coulomb gauge. Specifically, we write

$$H_{e-p} = \int \psi^\dagger [h_0 - \alpha Z(r)/r] \psi d^3r, \quad (3.1)$$

$$H_I = H_I^{(1)} + H_I^{(2)},$$

$$H_I^{(1)} = -e \int \psi^\dagger \vec{\alpha} \cdot \vec{A} \psi d^3r, \quad (3.2)$$

$$\begin{aligned} H_I^{(2)} &= \alpha \int \int \frac{d^3r_1 d^3r_2}{R_{12}} (\psi^\dagger \psi)_1 (\psi^\dagger \psi)_2 \\ &\quad - \alpha \int \psi^\dagger \frac{Y(r)}{r} \psi d^3r, \end{aligned} \quad (3.3)$$

with $R_{12} = |\vec{r}_1 - \vec{r}_2|$.

The field operator ψ is expanded in the complete set of orbitals of Eq. (2.1). The transverse electromagnetic vector potential \vec{A} is expanded in

TABLE I. Theoretical transition rates w for the $M1$ decay $2^3S_1 \rightarrow 1^1S_0$ in the He isoelectronic sequence. Results of the present calculation are compared with Drake's (Ref. 3, p. 913) previous theoretical values. Numbers in parentheses represent powers of 10.

Z	w (sec $^{-1}$)	w_{Drake} (sec $^{-1}$)	Z	w (sec $^{-1}$)	w_{Drake} (sec $^{-1}$)
2	1.253(-4)	1.272(-4)	21	2.338(7)	2.275(7)
3	2.037(-2)	2.039(-2)	22	3.767(7)	3.656(7)
4	5.638(-1)	5.618(-1)	23	5.939(7)	5.751(7)
5	6.731(0)	6.695(0)	24	9.183(7)	8.870(7)
6	4.887(1)	4.856(1)	25	1.395(8)	1.344(8)
7	2.551(2)	2.532(2)	26	2.084(8)	2.002(8)
8	1.052(3)	1.044(3)	30	9.023(8)	
9	3.640(3)	3.608(3)	35	4.383(9)	
10	1.098(4)	1.087(4)	40	1.729(10)	
11	2.966(4)	2.935(4)	45	5.828(10)	
12	7.327(4)	7.243(4)	50	1.737(11)	
13	1.680(5)	1.658(5)	55	4.694(11)	
14	3.614(5)	3.563(5)	60	1.171(12)	
15	7.365(5)	7.251(5)	65	2.732(12)	
16	1.432(6)	1.408(6)	70	6.032(12)	
17	2.672(6)	2.622(6)	75	1.272(13)	
18	4.808(6)	4.709(6)	80	2.577(13)	
19	8.377(6)	8.187(6)	85	5.054(13)	
20	1.418(7)	1.383(7)	90	9.639(13)	

electric and magnetic multipoles.

The lowest-order contribution to the decay rate arising from the first-order S -matrix element $S^{(1)}$ is illustrated by the Feynman diagram of Fig. 3(a). The remaining diagrams of Fig. 3 illustrate terms of importance in the third-order S matrix $S^{(3)}$. The diagrams of Figs. 3(b)–3(e) illustrate third-order terms contributed by the electron-electron Coulomb interaction. The influence of the DHF counter term is illustrated by the two diagrams 3(c') and 3(e'). It will be shown later that the two DHF counter terms cancel identically the Coulomb contributions of diagrams 3(c) and 3(e). The remaining Coulomb diagrams, 3(b) and 3(d), represent a residual

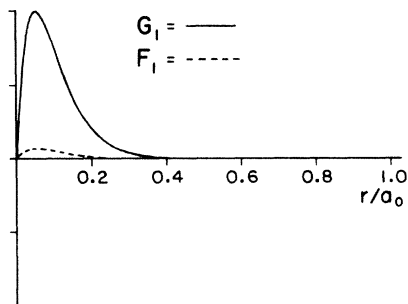


FIG. 1. Radial DHF wave functions for the $1s_{1/2}$ orbital with $Z=20$. The functions $G_1(r)$ and $F_1(r)$ are the large and small components of the corresponding orbital.

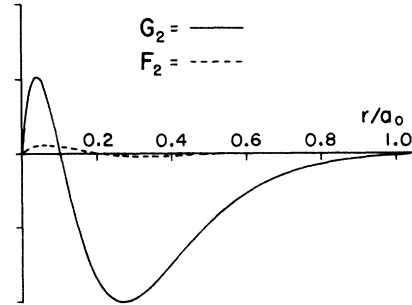


FIG. 2. Radial DHF wave functions for the $2s_{1/2}$ orbital with $Z=20$. The functions $G_2(r)$ and $F_2(r)$ are the large and small components of the corresponding orbital.

correlation effect. The diagrams of Figs. 3(b'')–3(e'') represent third-order effects due to the exchange of one transverse photon which contribute to the same order in both α and αZ as the terms of Figs. 3(b) and 3(d).

That part of the electron-electron interaction included in ψ will be called a "screening" correction. The remaining parts of the electron-electron Coulomb interaction, accounted for by 3(b) and 3(d), will be called "correlation" corrections. In Sec. IV we determine the screened decay rates from Fig. 3(a). We evaluate the correlation and transverse photon corrections in Sec. V.

There are, of course, other contributions to $S^{(3)}$ which could be included with those illustrated

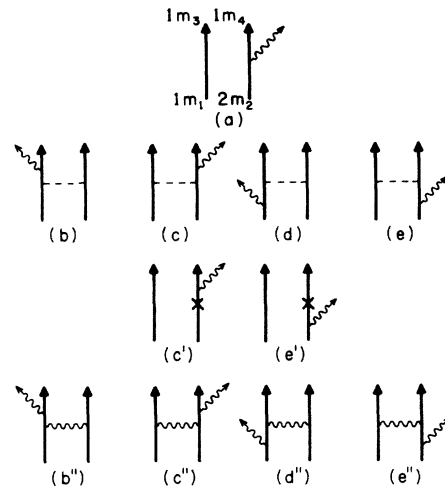


FIG. 3. Heavy lines represent a bound electron; the electron quantum numbers, explicitly represented on the first-order diagram (a), are understood to occur in the same position on the remaining diagrams. The electron-electron Coulomb interaction is illustrated by the dashed lines in diagrams of the second row. The cross in the diagrams of the third row indicate the DHF counter term. The wavy lines, as usual, represent a transverse photon.

in Fig. 3; they are vacuum-polarization and self-energy terms. By limiting ourselves to the diagrams of Fig. 3 we avoid those difficulties which require the use of damping theory,¹¹ or similar techniques. In evaluating the transverse-photon-exchange diagrams we drop retardation, which contributes to the same order as the vacuum-polarization and self-energy terms already omitted.

IV. FIRST-ORDER DECAY-RATE CALCULATION

The initial and final two-electron states are described by the interaction-representation state vectors

$$|2^3S_1\rangle = \sum_{m_1 m_2} C(\frac{1}{2}\frac{1}{2}1, m_1 m_2 m) |1s_{1/2}m_1, 2s_{1/2}m_2\rangle, \quad (4.1)$$

$$|1^1S_0\rangle = \frac{1}{\sqrt{2}} \sum_{m_3 m_4} C(\frac{1}{2}\frac{1}{2}0, m_3 m_4 0) |1s_{1/2}m_3, 1s_{1/2}m_4\rangle.$$

In Eqs. (4.1) the Clebsch-Gordan coefficients assure that the states have the correct angular momentum, while the factor $\sqrt{2}$ in the ground state is for normalization purposes. The z angular momentum of the 2^3S_1 state is m .

We expand the electromagnetic vector potential in multipoles as mentioned previously. The relation between the multipole expansion and the usual plane-wave expansion is given by

$$\hat{\epsilon} e^{i\vec{k}\cdot\vec{r}} = \sum_{JM\lambda} C_{JM}^\lambda(\hat{k}, \hat{\epsilon}) \bar{A}_{JM}^\lambda(kr), \quad (4.2a)$$

$$C_{JM}^\lambda(\hat{k}, \hat{\epsilon}) = 4\pi i^{J-\lambda} \bar{Y}_{JM}^\lambda(\hat{k}) \cdot \hat{\epsilon}. \quad (4.2b)$$

Definitions of the multipole vectors \bar{A}_{JM}^λ and the vector spherical harmonics \bar{Y}_{JM}^λ are found in Ref. 12; the vector $\hat{\epsilon}$ is the transverse polarization vector. In the expansion of Eqs. (4.2a) $\lambda=0$ and 1 refer to magnetic and electric multipoles, respectively, while J and M are the photon-angular-momentum quantum numbers. Conservation of angular momentum and parity limit the sum in Eq. (4.2a) to a single magnetic dipole term with $\lambda=0$, $J=1$, and $M=m$.

In writing down the S -matrix element it is convenient to extract the polarization-dependent coefficient $C_{1m}^0(\hat{k}, \hat{\epsilon})$ in addition to the usual kinematic factors. We write

$$S = -2\pi i \frac{e}{(2\omega V)^{1/2}} \delta(\omega - \epsilon_2 + \epsilon_1) C_{1m}^{0*}(\hat{k}, \hat{\epsilon}) M. \quad (4.3)$$

Summing over polarization directions and integrating over photon angles we find that the transition rate w is given by

$$w = 8\pi\alpha |M|^2. \quad (4.4)$$

The matrix element M is conveniently decomposed by removing the initial- and final-state Clebsch-Gordan coefficients

$$M = \sqrt{2} \sum C(\frac{1}{2}\frac{1}{2}1; m_1 m_2 m) C(\frac{1}{2}\frac{1}{2}0; m_3 m_4 0) T. \quad (4.5)$$

The contribution to T which arises in first order from Fig. 3(a) is

$$T^{(1)} = -\delta_{m_1 m_3} \int u_{1m_4}^\dagger \bar{A}_{1m}^{0*} \cdot \vec{a} u_{2m_2} d^3r. \quad (4.6)$$

Performing the angular integration in Eq. (4.6) and substituting into Eq. (4.5) we find that the first-order contribution to M is given by

$$M^{(1)} = (i/\sqrt{3}\pi) Q_a. \quad (4.7)$$

The radial integral Q_a is expressed in terms of the radial functions of orbitals 1 and 2 by

$$Q_a = \int j_1(kr)(G_1 F_2 + F_1 G_2) dr, \quad (4.8)$$

where $j_1(kr)$ is a spherical Bessel function of order 1.

Combining Eqs. (4.5) and (4.7) we find a simple first-order expression for the decay rate:

$$w^{(1)} = \frac{8}{3} \alpha \omega Q_a^2. \quad (4.9)$$

If we use Coulomb wave functions rather than screened DHF wave functions to evaluate Eq. (4.8) and drop $(\alpha Z)^2$ relativistic corrections, we are led to the approximate result

$$w^{(1)} \approx 1.664Z^{10} \times 10^{-6} \text{ sec}^{-1}. \quad (4.10)$$

Using the form suggested by Eq. (4.10) to parameterize the decay rate we write

$$w = 1.664F(Z)Z^{10} \times 10^{-6} \text{ sec}^{-1}. \quad (4.11)$$

The contribution $F^{(1)}(Z)$ to the "form factor" $F(Z)$ determined in lowest-order perturbation theory from Eq. (4.9) is listed in Table II. The corresponding first-order decay rates are found to be substantially smaller than the rates calculated in Ref. 3, especially for the lightest elements. This discrepancy disappears, however, when third-order contributions are included in the calculation.

V. THIRD-ORDER CORRELATION AND TRANSVERSE PHOTON CORRECTIONS TO THE DECAY RATE

To illustrate the technique used in the third-order calculation of the transition matrix element T let us consider the Feynman diagram of Fig. 3(d). We may immediately write

$$T_d^{(3)} = \alpha \int \int \int \frac{d^3 r_1 d^3 r_2 d^3 r_3}{R_{13}} \times [u_{1m_3}^\dagger S_F(\vec{r}_1, \vec{r}_2, \epsilon_1 - \omega) \vec{A}_{1m}^{0*} \cdot \vec{\alpha} u_{1m_1}]_{12} \times (u_{1m_4}^\dagger u_{2m_2})_3, \quad (5.1)$$

where $R_{13} = |\vec{r}_1 - \vec{r}_3|$, and where the Feynman propagator S_F is given by

$$S_F(\vec{r}_1, \vec{r}_2, \epsilon) = \sum_{\epsilon_n > 0} \frac{u_n(\vec{r}_1) u_n^\dagger(\vec{r}_2)}{\epsilon_n - \epsilon - i\eta} + \sum_{\epsilon_n < 0} \frac{u_n(\vec{r}_1) u_n^\dagger(\vec{r}_2)}{\epsilon_n - \epsilon + i\eta}. \quad (5.2)$$

The orbitals $u_n(r)$ are solutions to the DHF equations (2.1). To avoid a direct evaluation of Eq. (5.2) we make use of a technique developed by Brown *et al.*¹³ The technique consists of introducing a perturbed orbital

$$w^d(\vec{r}_1) = \int S_F(\vec{r}_1, \vec{r}_2, \epsilon_1 - \omega) \vec{A}_{1m}^{0*} \cdot \vec{\alpha} u_{1m_1}(\vec{r}_2) d^3 r_2 \quad (5.3)$$

which satisfies an inhomogeneous DHF equation,

$$[h_0 - \alpha Z(r)/r - \epsilon_1 + \omega] w^d = \vec{A}_{1m}^{0*} \cdot \vec{\alpha} u_{1m_1}. \quad (5.4)$$

The inhomogeneous DHF equation (5.4) can be decomposed into angular momentum states and reduced to a set of coupled radial differential equations. The techniques used for carrying out the angular decomposition are discussed, for example, by Feiock and Johnson.¹⁴

Specifically we write

$$w^d = \sum_{\bar{\kappa} \bar{m}} C_{\bar{\kappa} \bar{m}} w_{\bar{\kappa} \bar{m}}^d, \quad (5.5)$$

where the perturbations $w_{\bar{\kappa} \bar{m}}^d$ are limited by angular

TABLE II. Form factor $F(Z)$ defined by $w = 1.664 F(Z) \times Z^{10} \times 10^{-6} \text{ sec}^{-1}$. The lowest-order contribution $F^{(1)}(Z)$ is tabulated along with the final value $F(Z)$. The validity of the perturbation approach for large Z can be judged by comparing $F^{(1)}(Z)$ and $F(Z)$.

Z	$F^{(1)}(Z)$	$F(Z)$	Z	$F^{(1)}(Z)$	$F(Z)$
2	0.0350	0.0736	25	0.8343	0.8790
4	0.2291	0.3231	30	0.8794	0.9183
6	0.3879	0.4857	35	0.9201	0.9547
8	0.4983	0.5890	40	0.9596	0.9909
10	0.5775	0.6596	45	0.9998	1.0286
12	0.6369	0.7112	50	1.0423	1.0691
14	0.6833	0.7509	60	1.1392	1.1633
16	0.7209	0.7827	70	1.2607	1.2834
18	0.7523	0.8093	80	1.4202	1.4424
20	0.7793	0.8321	90	1.6385	1.6614

momentum and parity selection rules to have quantum numbers $\bar{\kappa} = -1, +2$ (corresponding to $s \rightarrow s$ and $s \rightarrow d$ perturbations), and $\bar{m} = m_1 - m = -m_2$. The expansion coefficients $C_{\bar{\kappa} \bar{m}}$ are given in terms of $j = |\bar{\kappa}| - \frac{1}{2}$ by

$$C_{\bar{\kappa} \bar{m}} = (-1)^{j+1/2} [(2j+1)/4\pi]^{1/2} \times C(\bar{j} \frac{1}{2}, \frac{1}{2} 0 \frac{1}{2}) C(\bar{j} 1 \frac{1}{2}, \bar{m} m m_1). \quad (5.6)$$

We may further decompose $w_{\bar{\kappa} \bar{m}}^d$ in a spherical basis as

$$w_{\bar{\kappa} \bar{m}}^d = \frac{1}{r} \left(i S_{\bar{\kappa}}^d(r) \Omega_{\bar{\kappa} \bar{m}}(\hat{r}) \right) \quad (5.7)$$

from which follows the radial differential equations

$$\left(\frac{d}{dr} - \frac{\bar{\kappa}}{r} \right) T_{\bar{\kappa}}^d + \left(m - \epsilon_1 + \omega - \frac{\alpha Z(r)}{r} \right) S_{\bar{\kappa}}^d = j_1(kr) F_1(r),$$

$$\left(\frac{d}{dr} + \frac{\bar{\kappa}}{r} \right) S_{\bar{\kappa}}^d + \left(m + \epsilon_1 - \omega + \frac{\alpha Z(r)}{r} \right) T_{\bar{\kappa}}^d = -j_1(kr) G_1(r). \quad (5.8)$$

The radial differential equations (5.8) together with the boundary conditions that $S_{\bar{\kappa}}^d$ and $T_{\bar{\kappa}}^d$ vanish for $r=0$ and for $r=\infty$ are suitable for numerical solution. We postpone further discussion until Sec. VI.

In terms of the perturbations w^d introduced above we can simplify Eq. (5.1) to

$$T_d^{(3)} = \alpha \int \int \frac{d^3 r_1 d^3 r_2}{R_{12}} (u_{1m_3}^\dagger w^d)_1 (u_{1m_4}^\dagger u_{2m_2})_2. \quad (5.9)$$

The angular decomposition of each term in the integrand can be introduced at this stage and the matrix element thereby reduced to radial integrals similar in form to the Slater integrals of atomic-structure calculations.¹⁵ Carrying out the calculations described above and substituting $T_d^{(3)}$ into Eq. (4.5) we find that Fig. 3(d) contributes to the third-order matrix element $M^{(3)}$ a term

$$M_d^{(3)} = -(i\alpha/\sqrt{3\pi}) Q_d, \quad (5.10)$$

where the Slater integral Q_d is given by

$$Q_d = \int \int \frac{dr_1 dr_2}{r_>} (S_{-1}^d G_1 + T_{-1}^d F_1)_1 (G_1 G_2 + F_1 F_2)_2. \quad (5.11)$$

It should be noted that only the perturbation with $\bar{\kappa} = -1$ ($s \rightarrow s$) contributes to Q_d .

An entirely similar procedure can be carried out for each of the Coulomb terms of Figs. 3(b)–3(e). The relevant formulas are collected in Appendix A.

The two DHF counter terms of Figs. 3(c') and 3(e') may also be reduced in terms of perturbed orbitals. For example, we find that the contribu-

tion from 3(e') can be written

$$T_e^{(3)} = -\alpha \delta_{m_1 m_3} \int u_{1m_4}^+ \frac{Y(r)}{r} w^e d^3 r, \quad (5.12)$$

where the perturbation w^e satisfies Eq. (A1e) of Appendix A. Carrying out the angular integration and making use of the definition of $Y(r)$ given in Eq. (2.2) we find that Fig. 3(e') contributes to $M^{(3)}$ a term

$$M_e^{(3)} = -(i\alpha/\sqrt{3\pi}) Q_e, \quad (5.13)$$

where the Slater integral Q_e is given in Eq. (A5) of Appendix A. The contribution $M_e^{(3)}$ is equal in magnitude and opposite in sign to the Coulomb term $M_e^{(3)}$.

The transverse-photon exchange diagrams of Figs. 3(b'') to 3(d'') are similarly evaluated in terms of the perturbed orbitals. The contribution of Fig. 3(d''), for example, reduces to Eq. (5.9) with the modification that the Coulomb interaction α/R_{12} is replaced by the Breit interaction

$$B_{12} = -(\alpha/2R_{12})(\vec{\alpha}_1 \cdot \vec{\alpha}_2 + \vec{\alpha}_1 \cdot \hat{R}_{12} \vec{\alpha}_2 \cdot \hat{R}_{12}). \quad (5.14)$$

The Breit operator follows from diagram 3(d'') after dropping retardation, an approximation which is consistent with the neglect of self-energy and vacuum-polarization corrections. Techniques for evaluating two-electron matrix elements of the Breit operator using DHF orbitals have been given by Grant, by Kim, and by Mann and Johnson.¹⁶ Making use of these techniques we find that the contribution of Fig. 3(d'') to $M^{(3)}$ is

$$M_{d''}^{(3)} = -(i\alpha/3\sqrt{3\pi}) Q_{d''}(-1), \quad (5.15)$$

where the magnetic Slater integral $Q_{d''}(\kappa)$ is listed in Eq. (A9d''). The argument κ of the magnetic Slater integral refers to the angular momentum quantum number of the perturbed orbital $w_{\kappa m}^d$.

To summarize, we write the entire third-order contribution to M as

$$\begin{aligned} M^{(3)} = & -(i\alpha/\sqrt{3\pi}) \\ & \times [Q_b + Q_c - \frac{1}{9}Q_b''(-1) + \frac{4}{9}Q_b''(2) + \frac{1}{9}Q_c''(-1) \\ & - \frac{4}{9}Q_c''(2) + \frac{1}{3}Q_{d''}(-1) - \frac{1}{3}Q_e''(-1)]. \end{aligned} \quad (5.16)$$

In writing down Eq. (5.16) we have omitted the terms from diagrams 3(c) and 3(c') and from 3(e) and 3(e'), which are shown to cancel in Appendix A. This cancellation was not unexpected; it occurs because screening effects represented by diagrams 3(c) and 3(e) are already included in Q_a ; the counter term introduced in the interaction Hamiltonian assures that the interaction is not again counted in the perturbation expansion. The remaining Coulomb terms of Figs. 3(b) and 3(d) represent

the "correlation" corrections referred to earlier.

Adding the first- and third-order contributions to M we have our final expression for the transition rate,

$$\begin{aligned} w = & \frac{8}{3} \alpha \omega Q_a^2 (1 + 2\Delta), \\ \Delta = & M^{(3)}/M^{(1)}. \end{aligned} \quad (5.17)$$

As we show in Sec. VI, the third-order matrix element $M^{(3)}$ is of order $\alpha(\alpha Z)^3$, while the first-order matrix element $M^{(1)}$ is of order $(\alpha Z)^1$. The correction Δ is, therefore, of order Z^{-1} , as mentioned in the Introduction. Parametrizing the decay rate according to Eq. (4.11) we find

$$F(Z) = F^{(1)}(Z)(1 + 2\Delta), \quad (5.18)$$

where $F^{(1)}(Z)$ is determined from the first-order calculation. The relatively small difference between $F(Z)$ and $F^{(1)}(Z)$ for large Z seen in Table II serves as a measure of validity of the perturbation approach employed above.

VI. EVALUATION OF THE THIRD-ORDER MATRIX ELEMENT

In this section we discuss some of the details connected with the evaluation of the third-order matrix element.

Let us first consider the inhomogeneous differential equations for the perturbations introduced in Eqs. (5.8) and (A2). Applying the Pauli approximation to these inhomogeneous equations we obtain approximate nonrelativistic solutions. These approximate solutions are given by

$$\begin{aligned} \begin{pmatrix} S_{\kappa}^b \\ T_{\kappa}^b \end{pmatrix} &= \begin{pmatrix} S_{\kappa}^c \\ T_{\kappa}^c \end{pmatrix} \approx -\frac{1}{2m} \begin{pmatrix} G_1 \\ F_1 \end{pmatrix} \delta_{\kappa, -1} - \frac{\omega r}{6m} \begin{pmatrix} F_1 \\ G_1 \end{pmatrix}, \\ \begin{pmatrix} S_{\kappa}^d \\ T_{\kappa}^d \end{pmatrix} &\approx \frac{1}{2m} \begin{pmatrix} G_1 \\ F_1 \end{pmatrix} \delta_{\kappa, -1} - \frac{\omega r}{6m} \begin{pmatrix} F_1 \\ G_1 \end{pmatrix}, \\ \begin{pmatrix} S_{\kappa}^e \\ T_{\kappa}^e \end{pmatrix} &\approx \frac{1}{2m} \begin{pmatrix} G_2 \\ F_2 \end{pmatrix} \delta_{\kappa, -1} - \frac{\omega r}{6m} \begin{pmatrix} F_2 \\ G_2 \end{pmatrix}. \end{aligned} \quad (6.1)$$

The leading terms on the right-hand sides of Eqs. (6.1), which are independent of photon energy, are easily seen to cancel in the third-order matrix element. To avoid numerical complications we subtract the leading terms from S_{κ} and T_{κ} and modify the inhomogeneous equations accordingly. The second terms on the right of Eqs. (6.1) represent the "proper" nonrelativistic effects to lowest order in αZ . Examining these residual terms we find that [relative to the large component $G_1(r)$ of the unperturbed orbital] S_{κ} is of order $(\alpha Z)^2$ and T_{κ} is of order αZ .

Using these nonrelativistic order-of-magnitude estimates for the size of S_{κ} and T_{κ} one sees that the Slater integrals Q_{ν} (both electric and mag-

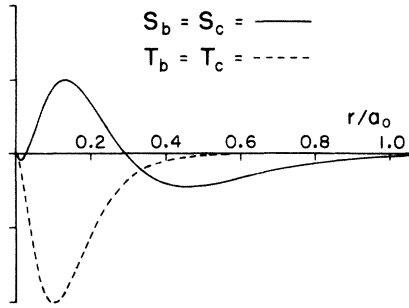


FIG. 4. Solution to the perturbed orbital radial equations for $Z=20$. The solid lines represent the "large" component of the perturbed orbital corresponding to diagrams 3(b) and 3(c), while the dashed lines give the "small" component. The approximate behavior $T^{(b),(c)} \approx -\omega r G_1/6m$ is evident on comparison with Fig. 1.

netic types) defined in Appendix A are all of order $(\alpha Z)^3$ as claimed previously.

After subtracting out the leading terms of Eqs. (6.1) the inhomogeneous radial equations (A2) are solved numerically. Graphs of the solutions for the perturbed orbitals are given in Figs. 4–6, for the special case $Z=20$ and $\kappa=-1$. Comparing these perturbed orbitals with the unperturbed orbitals of Figs. 1 and 2 one can see that the solutions behave approximately as predicted by Eq. (6.1).

Once the perturbed orbitals are obtained by numerical integration of the radial equations, the Slater integrals of Eqs. (A5) and (A6) are carried out numerically and combined according to Eqs. (5.16) and (5.17) to give the transition rate.

In carrying out the numerical work advantage is taken of the fact that the magnetic contributions of $Q_{b''}(-1)$ and $Q_{b''}(2)$ cancel to order $(\alpha Z)^3$. The residual difference is thus of order $(\alpha Z)^5$ and can be neglected along with the self-energy and vacuum-polarization terms. The same cancellation occurs between $Q_{c''}(-1)$ and $Q_{c''}(2)$ and these terms

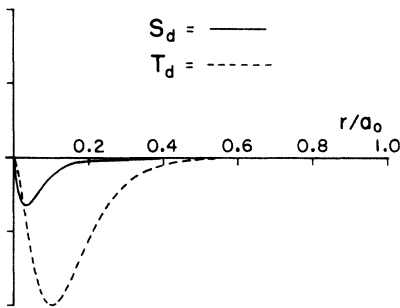


FIG. 5. Solution to the perturbed orbital radial equation for diagram 3(d). The approximate nonrelativistic behavior $T^{(d)} \approx -\omega r G_1/6m$ is evident on comparison with Fig. 1.

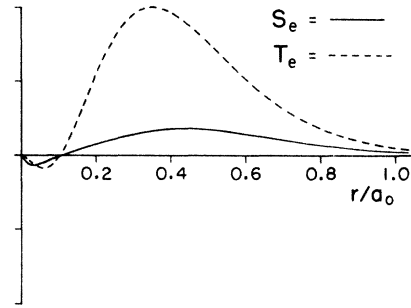


FIG. 6. Behavior of the perturbed orbital radial functions for diagram 3(e). The approximate nonrelativistic behavior $T^{(e)} \approx -\omega r G_2/6m$ is seen on comparison with Fig. 2.

are also dropped. Since these two magnetic integrals, $Q_{b''}(2)$ and $Q_{c''}(2)$, are the only terms involving $\bar{\kappa}=2$ it is unnecessary to solve Eqs. (A2) for $\bar{\kappa}=2$.

APPENDIX

Following the procedure outlined previously in Sec. V we can introduce a perturbed orbital for each of the four diagrams 3(b)–3(e) of Fig. 3. The perturbed orbitals are labeled with a superscript to represent the corresponding diagram. We find

$$\begin{aligned} [h_0 - \alpha Z(r)/r - \epsilon_2]w^b &= \vec{\alpha} \cdot \vec{A}_{1m}^0 u_{1m_3} - \langle 2, m+m_3 | \vec{\alpha} \cdot \vec{A}_{1m}^0 | 1m_3 \rangle u_{2m+m_3}, \\ & \quad (A1b) \end{aligned}$$

$$\begin{aligned} [h_0 - \alpha Z(r)/r - \epsilon_1]w^c &= \vec{\alpha} \cdot \vec{A}_{1m}^0 u_{1m_4} - \langle 2, m+m_4 | \vec{\alpha} \cdot \vec{A}_{1m}^0 | 1m_4 \rangle u_{2m+m_4}, \\ & \quad (A1c) \end{aligned}$$

$$[h_0 - \alpha Z(r)/r - \epsilon_1 + \omega]w^d = \vec{A}_{1m}^{0*} \cdot \vec{\alpha} u_{1m_1}, \quad (A1d)$$

$$\begin{aligned} [h_0 - \alpha Z(r)/r - \epsilon_1]w^e &= \vec{A}_{1m}^{0*} \cdot \vec{\alpha} u_{2m_2} - \langle 1m_2 - m | \vec{A}_{1m}^{0*} \cdot \vec{\alpha} | 2m_2 \rangle u_{1m_2-m}. \\ & \quad (A1e) \end{aligned}$$

We can carry out an angular decomposition of each of these equations into a sum of terms corresponding to perturbations $(s-s)$ and $(s-d)$, labeled by angular momentum quantum numbers $\bar{\kappa}=-1$ and $\bar{\kappa}=2$, respectively.

The radial differential equations analogous to Eqs. (5.8) for the perturbation can be written

$$\begin{aligned} \left(\frac{d}{dr} - \frac{\bar{\kappa}}{r}\right)T_{\bar{\kappa}} + \left(m - \epsilon - \frac{\alpha Z(r)}{r}\right)S_{\bar{\kappa}} &= K_{\bar{\kappa}}^-, \\ \left(\frac{d}{dr} + \frac{\bar{\kappa}}{r}\right)S_{\bar{\kappa}} + \left(m + \epsilon + \frac{\alpha Z(r)}{r}\right)T_{\bar{\kappa}} &= -L_{\bar{\kappa}}^-. \end{aligned} \quad (A2)$$

The parameter ϵ takes on one of the values ϵ_2 , $\epsilon_1 - \omega$, or ϵ_1 , depending on the equation in question, while the inhomogeneous terms are given by

$$\begin{aligned} K_{\bar{\kappa}}^b &= K_{\bar{\kappa}}^c = j_1(kr)F_1(r) - Q_a G_2(r)\delta_{\bar{\kappa}, -1}, \\ L_{\bar{\kappa}}^b &= L_{\bar{\kappa}}^c = j_1(kr)G_1(r) - Q_a F_2(r)\delta_{\bar{\kappa}, -1}, \\ K_{\bar{\kappa}}^d &= j_1(kr)F_1(r), \\ L_{\bar{\kappa}}^d &= j_1(kr)G_1(r), \\ K_{\bar{\kappa}}^e &= j_1(kr)F_2(r) - Q_a G_1(r)\delta_{\bar{\kappa}, -1}, \\ L_{\bar{\kappa}}^e &= j_1(kr)G_2(r) - Q_a F_1(r)\delta_{\bar{\kappa}, -1}. \end{aligned} \quad (\text{A3})$$

The coefficient Q_a occurring above is just the first-order radial integral defined in Eq. (4.8).

Carrying out the details of the calculations outlined in Sec. V for the four diagrams 3(b)–3(d) we obtain

$$M_{b-e}^{(3)} = -(i\alpha/\sqrt{3\pi})(Q_b - Q_c + Q_d - Q_e), \quad (\text{A4})$$

where the Slater integrals Q_ν are given by

$$Q_b = \int \int \frac{dr_1 dr_2}{r_>} (S_{-1}^b G_1 + T_{-1}^b F_1)_1 (G_1 G_2 + F_1 F_2)_2, \quad (\text{A5b})$$

$$Q_c = \int \int \frac{dr_1 dr_2}{r_>} (S_{-1}^c G_2 + T_{-1}^c F_2)_1 (G_1^2 + F_1^2)_2, \quad (\text{A5c})$$

$$Q_d = \int \int \frac{dr_1 dr_2}{r_>} (S_{-1}^d G_1 + T_{-1}^d F_1)_1 (G_1 G_2 + F_1 F_2)_2, \quad (\text{A5d})$$

$$Q_e = \int \int \frac{dr_1 dr_2}{r_>} (S_{-1}^e G_1 + T_{-1}^e F_1)_1 (G_1^2 + F_1^2)_2. \quad (\text{A5e})$$

Similarly we find that diagrams for the two counter terms, Figs. 3(c') and 3(e'), give

$$M_{c'+e'}^{(3)} = -(i/\sqrt{3\pi})(Q_{c'} + Q_{e'}), \quad (\text{A6})$$

where

$$Q_{c'} = \alpha \int_0^\infty \frac{dr}{r} (S_{-1}^c G_2 + T_{-1}^c F_2) Y(r), \quad (\text{A7c'})$$

$$Q_{e'} = \alpha \int_0^\infty \frac{dr}{r} (S_{-1}^e G_1 + T_{-1}^e F_1) Y(r). \quad (\text{A7e'})$$

Making use of the definition of $Y(r)$ given in Eq. (2.3) we see that $Q_{c'} = \alpha Q_c$ and that $Q_{e'} = \alpha Q_e$, so that the corresponding matrix elements cancel identically.

Turning to the transverse photon diagrams of Figs. 3(b'')–3(d'') we find

$$\begin{aligned} M_{b''-e''}^{(3)} &= -(i\alpha/\sqrt{3\pi})[-\frac{1}{3}Q_{b''}(-1) + \frac{4}{3}Q_{b''}(2) \\ &\quad + \frac{1}{3}Q_{c''}(-1) - \frac{4}{3}Q_{c''}(2) \\ &\quad + \frac{1}{3}Q_{d''}(-1) - \frac{1}{3}Q_{e''}(-1)], \end{aligned} \quad (\text{A8})$$

where

$$\begin{aligned} Q_{b''}(\bar{\kappa}) &= \frac{1}{2}(\bar{\kappa}-1)^2 \int \int dr_1 dr_2 \frac{r_{<}}{r_>} (S_{\bar{\kappa}}^b F_1 + T_{\bar{\kappa}}^b G_1)_1 \\ &\quad \times (G_1 F_2 + F_1 G_2)_2, \end{aligned} \quad (\text{A9b''})$$

$$\begin{aligned} Q_{c''}(\bar{\kappa}) &= \frac{1}{2}(\bar{\kappa}-1)^2 \int \int dr_1 dr_2 \frac{r_{<}}{r_>} (S_{\bar{\kappa}}^c F_2 + T_{\bar{\kappa}}^c G_2)_1 \\ &\quad \times (2F_1 G_1)_2, \end{aligned} \quad (\text{A9c''})$$

$$\begin{aligned} Q_{d''}(\bar{\kappa}) &= \frac{1}{2}(\bar{\kappa}-1)^2 \int \int dr_1 dr_2 \frac{r_{<}}{r_>} (S_{\bar{\kappa}}^d F_1 + T_{\bar{\kappa}}^d G_1)_1 \\ &\quad \times (G_1 F_2 + F_1 G_2)_2, \end{aligned} \quad (\text{A9d''})$$

$$\begin{aligned} Q_{e''}(\bar{\kappa}) &= \frac{1}{2}(\bar{\kappa}-1)^2 \int \int dr_1 dr_2 \frac{r_{<}}{r_>} (S_{\bar{\kappa}}^e F_1 + T_{\bar{\kappa}}^e G_1)_1 \\ &\quad \times (2F_1 G_1)_2. \end{aligned} \quad (\text{A9e''})$$

*Research supported in part by the National Science Foundation under NSF Grant No. GP-32217X.

¹A. H. Gabriel and Carole Jordan, *Nature* **221**, 947 (1969); *Mon. Not. R. Astron. Soc.* **145**, 241 (1969); *Phys. Lett. A* **32**, 166 (1970); F. F. Freeman, A. H. Gabriel, B. B. Jones, and Carole Jordan, *Philos. Trans. R. Soc. Lond. A* **270**, 127 (1971).

²Hans R. Griem, *Astrophys. J.* **156**, L103 (1969); **161**, L155 (1970).

³G. W. F. Drake, *Phys. Rev. A* **3**, 908 (1971).

⁴G. Feinberg and J. Sucher, *Phys. Rev. Lett.* **26**, 681 (1971).

⁵I. L. Beigman and U. I. Safronova, *Zh. Eksp. Teor. Fiz.* **60**, 2045 (1971) [*Sov. Phys.—JETP* **33**, 1102 (1971)].

⁶Robert W. Schmieder and Richard Marrus, *Phys. Rev. Lett.* **25**, 1245 (1970); *Phys. Lett. A* **32**, 431 (1970); *Phys. Rev. A* **5**, 1160 (1972).

⁷H. W. Moos and J. R. Woodworth, *Phys. Rev. Lett.* **30**, 775 (1973).

⁸Harvey Gould, Richard Marrus, and Robert W. Schmieder, *Phys. Rev. Lett.* **31**, 504 (1973).

⁹C. L. Cocke, B. Curnutte, and R. Randall, *Phys. Rev. Lett.* **31**, 507 (1973).

¹⁰W. H. Furry, *Phys. Rev.* **81**, 115 (1951).

¹¹W. Heitler, *Proc. Camb. Philos. Soc.* **37**, 291 (1941).

¹²A. I. Akhiezer and V. B. Berestetskii, *Quantum Electrodynamics* (Interscience, New York, 1965), Chap. 1.

¹³G. E. Brown, R. E. Peierls, and J. B. Woodward, *Proc. R. Soc. A* **227**, 51 (1954).

¹⁴F. D. Feiock and W. R. Johnson, *Phys. Rev.* **187**, 39 (1969).

¹⁵John C. Slater, *Quantum Theory of Atomic Structure* (McGraw-Hill, New York, 1960), Vol. I, Chap. 14.

¹⁶I. P. Grant, *Proc. R. Soc. A* **262**, 555 (1961); *Adv. Phys.* **19**, 747 (1970); Y. K. Kim, *Phys. Rev.* **154**, 17 (1967); Joseph B. Mann and Walter R. Johnson, *Phys. Rev. A* **4**, 41 (1971).